NUCLEAR INSTRUMENTS AND METHODS **22** (1963) 189–200; NORTH-HOLLAND PUBLISHING CO.

PARTICLE IDENTIFICATION BY PULSE SHAPE DISCRIMINATION IN THE p-i-n TYPE SEMICONDUCTOR DETECTOR

C. A. J. AMMERLAAN, R. F. RUMPHORST and L. A. CH. KOERTS

Institute for Nuclear Physics Research, Amsterdam

Received 3 October 1962

When an ionizing particle enters a semiconductor radiation detector a voltage pulse is produced. The final pulse height is determined by the particle energy, while the range of the particle affects the shape of the pulse. The voltage pulse therefore contains information about the particle type. In the present paper the pulse height at a fixed time during the pulse rise time, is used as the range dependent quantity. A two-dimensional display of this quantity versus the energy of the particle showed that separation could be obtained between deuterons and α-particles with energies in the range from 8 to 26 MeV.

Calculations have been made on this effect based on the results of a pulse shape analysis. The agreement between the experimental and the calculated data proves that the theoretical picture is quite adequate.

1. Introduction

The experiments, to be described in this paper, were performed with the p-i-n type semiconductor detector, also known as the lithium drifted counter. The detector consists of essentially three parts, which are:

a) a low resistivity p-type, boron doped, region;
b) a region which is intrinsic at room temperature;
c) an n-type, heavily lithium doped, region.

When this p-i-n structure is reverse biased the entire voltage is developed across the very high resistivity intrinsic material. This material is the sensitive part of the detector. The electrical situation in the p-i-n detector, sometimes called solid state ionization chamber, is analogous to that existing in the gasfilled ionization chamber. A few important differences between these two detectors are the energy needed for the creation of a charge pair, the mobilities of the free charges and the density of the stopping medium.

An ionizing particle, incident on the detector, creates electrons and holes in the semiconductor material. These free charges are separated by the external field, thereby producing a voltage signal on the electrodes. The rise time of this signal will depend on the time needed for the collection of the charge, which in its turn is dependent on the distance to be traversed by the charge carriers. The pulse rise time will therefore depend on the range of the particle. This means that from the voltage pulse a quantity can be derived that in some way represents the range of the particle.

On the other hand the final pulse height depends linearly on the energy, which is lost by the particle in the detector. The voltage pulse therefore contains information about both the energy and the range of the particle. Since the nature of a particle is determined by these two quantities, the particle type can be deduced from an adequate pulse treatment.

The next paragraph gives a theoretical pulse analysis; the result shows the expected dependence of the signal height on time, energy and range (fig. 1). In § 3 the method used for the particle identification is discussed. The experimental set-up, beam arrangement, detector properties and electronic equipment, is described in § 4. In § 5 the experimental and calculated results are given in the figs. 6 to 10 and 12 to 14. The last paragraph which is devoted to a discussion of the results also contains some supplementary information.

2. Pulse Shape Analysis

A list of symbols used in this paragraph is given together with their definitions:

x : position coordinate along the detector axis, $x = 0$ at the detector surface (fig. 4).;
W : thickness of the intrinsic region of the detector;

R : range of the incident particle in the detector, i.e. in Si;

ρ : reduced range, $\rho = R/W$;

a,b: constants appearing in the range-energy relation;

A : mass number of the incident particle;

Z : charge number of the incident particle;

V : reverse bias of the detector;

F : electric field in the sensitive detector region, $F = V/W$;

μ_e : mobility of electrons in silicon;

μ_h : mobility of holes in silicon;

v_e : velocity of the electrons during their collection, $v_e = \mu_e F$;

v_h : velocity of the holes during their collection, $v_h = \mu_h F$;

t : time;

$t_{t,e}$: transit time of electrons through the detector, $t_{t,e} = W^2/\mu_e V$;

τ : reduced time, $\tau = t/t_{t,e}$;

E_i : energy of the incident particle;

E_d : energy loss of the particle in the detector;

E_e : pulse height, due to the movement of electrons;

E_h : pulse height, due to the movement of holes;

ε_e : reduced pulse height, due to the movement of electrons, $\varepsilon_e = E_e/E_i$;

ε_h : reduced pulse height, due to the movement of holes, $\varepsilon_h = E_h/E_i$;

ε : reduced total pulse height, $\varepsilon = \varepsilon_e + \varepsilon_h$.

It may be remarked that the same symbol E is used for pulse height and energy. This is justified by the fact that pulse heights represent an energy and occur only when normalised to the proper energy scale.

In the derivation of the pulse shape formulas several assumptions have to be made, which limit the validity of the results. These assumptions are given below, preceding the proper derivation of the formulas:

a. The mobilities of electrons and holes are independent of the electric field.

b. The electric field is constant over the whole intrinsic region. By this assumption, and also by the range-energy dependence to be used, the present analysis differs from that given by Tove and Falk[1]) for the p-n junction detector.

c. The particles enter the detector on the p-side. This is the electrically negative side of the detector, to which the created holes will move (fig. 4).

d. The direction of all incident particles is perpendicular to the detector surface. The particles will make tracks inside the detector which are parallel to the electric field. This situation is usually not encountered in the work with the ionization chamber.

e. The contribution to the signal, arising from holes, which have diffused from the insensitive n-type region at the back of the detector to the intrinsic region, can be neglected.

f. If there is an insensitive p-type layer, window-layer, in front of the detector no contribution to the signal from diffused electrons is experienced.

g. During the collection time no charge is lost by recombination or trapping.

h. The original charge distribution is not disturbed by diffusion.

i. The relationship between range and energy of a particle can be written as $R = aE_i^b$.

j. $\mu_e = 3\mu_h$.

The derivation of the pulse shape formula proceeds along the following lines. When a charged particle enters a semiconductor detector energy is lost among other things by the creation of electron-hole pairs. The mean energy, needed for the creation of such a pair, is independent of the particle energy. This implies that the density of the charge distribution along the particle track will be proportional to the energy loss of the particle per unit length.

The energy loss per unit length is derived from the range-energy relation of the particle concerned in silicon. In this analysis an empirical range-energy relation of the type $R = aE_i^b$ is used, giving rise to the following expression for $\mathrm{d}E/\mathrm{d}x$:

$$\frac{\mathrm{d}E}{\mathrm{d}x} = -\frac{1}{a^{1/b}b(R-x)^{(b-1)/b}}.$$

The value of b can be determined from the slope of the experimental range-energy curves on log-log paper. In the actual calculations for protons, deuterons and α-particles with energies between 5 and 50 MeV the value $b = 1.73$ was considered to

[1]) P. A. Tove and K. Falk, Nucl. Instr. and Meth. **12** (1961) 278.

be the best. The constant a was then found to have the following values:

$a = 12$, $R = 12 \quad E_i^{1.73}$, for protons

$a = 7.23$, $R = 7.23\, E_i^{1.73}$, for deuterons

$a = 1.09$, $R = 1.09\, E_i^{1.73}$, for α-particles.

The electron-hole pairs are created all at the time $t = 0$, when the particle is stopped in the detector. Because of the external electric field F, the holes created in the intrinsic region acquire a constant drift velocity $v_h = \mu_h F = \mu_h V/W$ in the direction of the negative p-type front layer. The first holes, created at $x = 0$, reach the front electrode at $t = 0$; the last ones, which are created at the end of the particle track $x = R$, arrive at the electrode at $t = RW/\mu_h V$. The electrons will move with constant velocity $v_e = \mu_e F = \mu_e V/W$ toward the positive back contact. The first electrons reach this electrode at the time $t = W(W - R)/\mu_e V$. The last electrons, which arrive at the electrode, are created at the position $x = 0$. These electrons have to traverse the whole detector thickness W, which takes the electron transit time $t_{t,e} = W^2/\mu_e V$.

In the case of constant charge a voltage pulse is produced. During their collection the electrons and holes are separated. The resulting change in space charge distribution causes a voltage pulse on the signal electrode of the detector. The height of the pulse, induced by one electron or hole, is proportional to the fraction of the junction thickness W traversed by that charge carrier. The total pulse height at the time t is obtained by integrating from $t = 0$ to that time the contributions from all electrons and holes.

The results of these calculations are given below. Although the preceeding text is essentially devoted to the case of particles which are stopped in the detector, calculations have also been made for particles which pass through the detector, giving up in the detector only part of their energy.

For the case $R \leqq W$ the results are:
Signal from the electrons:

$$0 \leqq t \leqq \frac{W(W-R)}{\mu_e V} : \quad E_e = E_i \frac{\mu_e V t}{W^2}$$

$$\frac{W(W-R)}{\mu_e V} \leqq t \leqq \frac{W^2}{\mu_e V} : \quad E_e = E_i \left\{ \frac{\mu_e V t}{W^2} - \frac{b}{b+1} \frac{R}{W} \left(1 - \frac{W}{R} + \frac{\mu_e V t}{RW} \right)^{(b+1)/b} \right\}$$

$$\frac{W^2}{\mu_e V} \leqq t : \quad E_e = E_i \left(1 - \frac{b}{b+1} \frac{R}{W} \right).$$

Signal from the holes:

$$0 \leqq t \leqq \frac{RW}{\mu_h V} : \quad E_h = E_i \frac{b}{b+1} \frac{R}{W} \left\{ 1 - \left(1 - \frac{\mu_h V t}{RW} \right)^{(b+1)/b} \right\}$$

$$\frac{RW}{\mu_h V} \leqq t : \quad E_h = E_i \frac{b}{b+1} \frac{R}{W}$$

These formulas can be presented in a more elegant way after the introduction of appropriate scales for the variables time, range and pulse height. The time t, relative to the electron transit time $W^2/\mu_e V$, is denoted by τ and called reduced time. Assuming $\mu_e = 3\mu_h$, the hole transit time $W^2/\mu_h V$ is given by the reduced time $\tau = 3$. The reduced range is defined by $\rho = R/W$. The reduced pulse heights for electrons and holes resp. are given by $\varepsilon_e = E_e/E_i$ and $\varepsilon_h = E_h/E_i$; they represent the pulse height relative to the pulse height corresponding to the incident particle energy. In general ε is a function of τ and ρ.

For the case $\rho \leqq 1$ the results are then:
Signal from the electrons:

$$0 \leqq \tau \leqq 1-\rho: \quad \varepsilon_e(\tau,\rho) = \tau$$

$$1-\rho \leqq \tau \leqq 1 \quad : \quad \varepsilon_e(\tau,\rho) = \tau - \frac{b}{b+1}\rho\left(1 - \frac{1-\tau}{\rho}\right)^{(b+1)/b}$$

$$1 \leqq \tau \quad : \quad \varepsilon_e(\tau,\rho) = 1 - \frac{b}{b+1}\rho .$$

Signal from the holes:

$$0 \leqq \tau \leqq 3\rho \quad : \quad \varepsilon_h(\tau,\rho) = \frac{b}{b+1}\rho\left\{1 - \left(1 - \frac{\tau}{3\rho}\right)^{(b+1)/b}\right\}$$

$$3\rho \leqq \tau \quad : \quad \varepsilon_h(\tau,\rho) = \frac{b}{b+1}\rho .$$

The pulse shapes of particles which pass through the detector are calculated by the same method. For this case, where $\rho \geqq 1$, the results are:
Signal from the electrons:

$$0 \leqq \tau \leqq 1: \quad \varepsilon_e(\tau,\rho) = \tau - \frac{b}{b+1}\rho\left\{\left(1 - \frac{1-\tau}{\rho}\right)^{(b+1)/b} - \left(1 - \frac{1}{\rho}\right)^{(b+1)/b}\right\}$$

$$1 \leqq \tau \quad : \quad \varepsilon_e(\tau,\rho) = 1 - \frac{b}{b+1}\rho\left\{1 - \left(1 - \frac{1}{\rho}\right)^{(b+1)/b}\right\}.$$

Signal from the holes:

$$0 \leqq \tau \leqq 3: \quad \varepsilon_h(\tau,\rho) = -\frac{\tau}{3}\left(1 - \frac{1}{\rho}\right)^{1/b} + \frac{b}{b+1}\rho\left\{1 - \left(1 - \frac{\tau}{3\rho}\right)^{(b+1)/b}\right\}$$

$$3 \leqq \tau \quad : \quad \varepsilon_h(\tau,\rho) = \rho\left\{\frac{b}{b+1} + \frac{1}{b+1}\left(1 - \frac{1}{\rho}\right)^{(b+1)/b} - \left(1 - \frac{1}{\rho}\right)^{1/b}\right\}$$

Since the boundaries for the validity of the above-mentioned formulas are fixed, in contrast with the case $\rho \leqq 1$ where they are range dependent, the formulas for $\varepsilon_e(\tau,\rho)$ and $\varepsilon_h(\tau,\rho)$ can be added to give the total pulse height $\varepsilon(\tau,\rho)$. Some simplification arises from this; for instance when $\tau \geqq 3$ the result becomes:

$$\rho \geqq 1,\ \tau \geqq 3: \quad \varepsilon(\tau,\rho) = 1 - \left(1 - \frac{1}{\rho}\right)^{1/b}$$

which implies:

$$E_d = E_i\left\{1 - \left(1 - \frac{1}{\rho}\right)^{1/b}\right\}.$$

In the actual calculations the value $b = 1.73$ has been used. Only the variables τ and ρ are left; τ defines the time, while the pulse shape is determined by ρ exclusively. The results are presented graphically in fig. 1.

In the figs. 2 and 3 some pulses obtained experimentally are reproduced. A set of five pulses, originating from deuterons with energies between 4 and 25 MeV, is shown in fig. 2. Fig. 3 gives a few pulses from α-particles with energies between 25 and 50 MeV. The pulse shape shows a behavior which verifies the predictions based on the ρ-values and the curves presented in fig. 1. This can be seen by a comparison of the deuteron and α-particle pulses at 25 MeV.

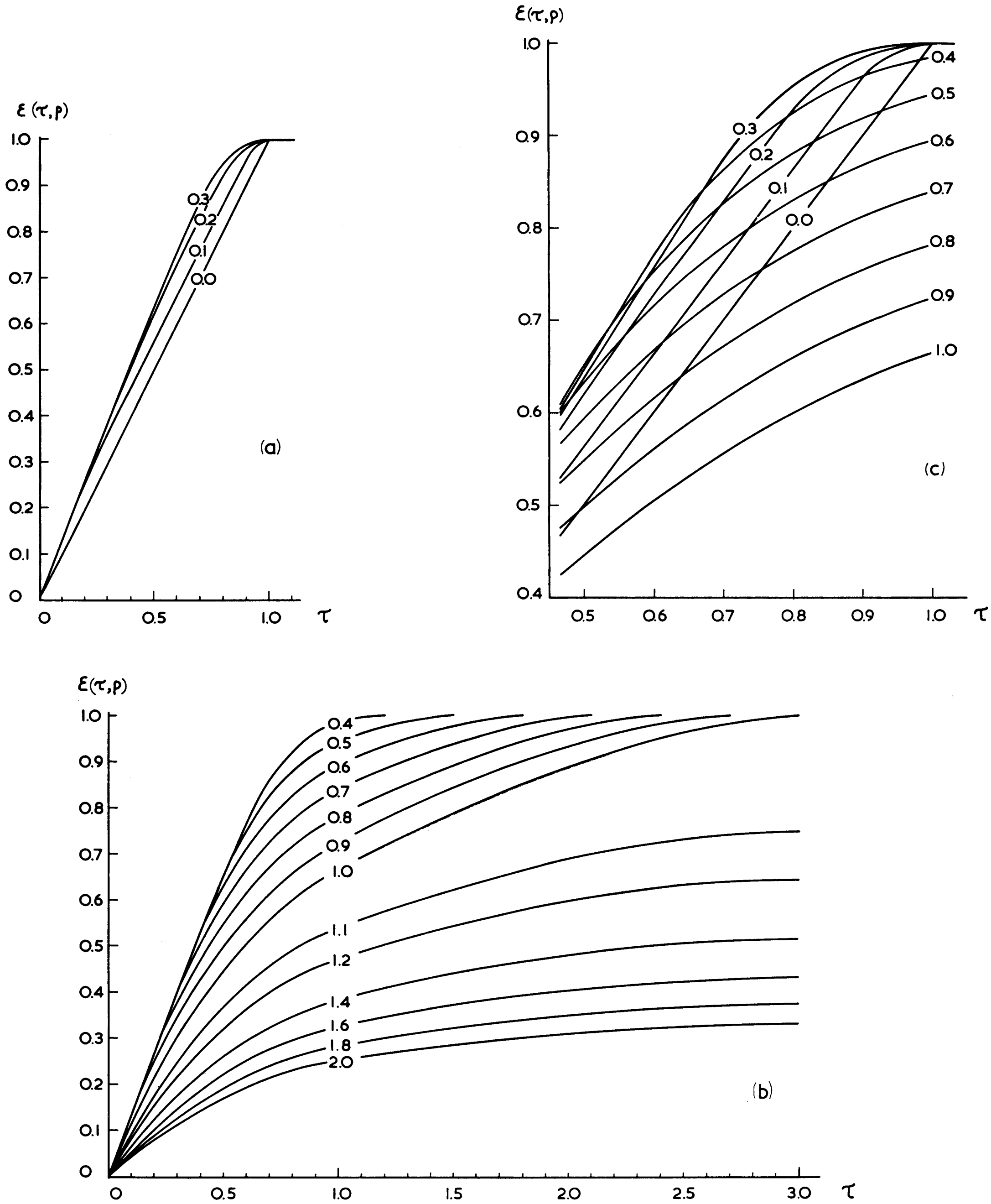

Fig. 1. Calculated pulse shapes for radiation incident normally on the p-side of a p-i-n detector. The curves are labelled with the appropriate value of the reduced range.

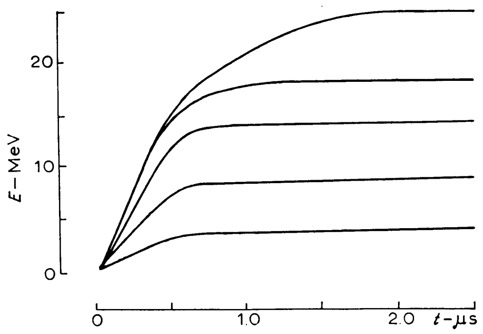

Fig. 2. Pulses of deuterons incident normally on the p-side of a p-i-n detector. $W = 2200\ \mu$m, $V = 42$ V, $t_{t,e} = 0.72\ \mu$s. Deuteron energies: 4, 9, 14, 18 and 25 MeV; corresponding ρ-values: 0.04, 0.14, 0.32, 0.49 and 0.86.

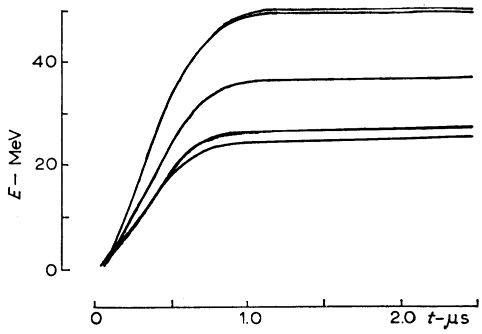

Fig. 3. Pulses of α-particles incident normally on the p-side of a p-i-n detector. $W = 2200\ \mu$m, $V = 42$ V, $t_{t,e} = 0.72\ \mu$s. α-particle energies: 25, 27, 36 and 50 MeV; corresponding ρ-values: 0.13, 0.15, 0.25 and 0.43.

3. Particle Identification Method

The nature of a particle is determined by specifying the range and the energy. Particle identification can therefore be obtained from the voltage pulse, produced by the particle in the detector, since this pulse contains information about both these quantities. The final pulse height, always reached at $\tau = 3$, is proportional to the energy lost in the detector, while, as is shown in the preceeding paragraph, the pulse shape depends on the range. In the particle identification method, described in this paper, the pulse height at a fixed time during the pulse rise time, is used as the range dependent quantity. Some considerations concerning the choice of this fixed time, called t_{cl}, are:

a. The pulse height for any $\tau \geqq 1$ is not able to discriminate between ρ-values in the range $0 \leqq \rho \leqq \frac{1}{3}$ (fig. 1a).

b. The pulse height for all times $0 < \tau < 1$ depends on ρ.

c. At the time $\tau = 0$ the slope of the pulse shape curves, $(\partial\varepsilon/\partial\tau)_{\tau=0}$, is equal to $\frac{4}{3}$, irrespective of ρ. For small times the variations with ρ in the pulse height are due only to differences in the second derivative; consequently they are small.

For the purpose of particle identification the region of primary interest centres around $\tau = \frac{3}{4}$, where the pulse height is most sensitive to the reduced range ρ. This region is drawn on enlarged scale in fig. 1c. The same conclusion can also be seen from an inspection of fig. 11, which gives the dependence of ε on ρ for various values of τ.

The particle identification depends on the pulse height at the time t_{cl}, abbreviated to E_{cl}. A two-dimensional display of E_{cl} versus the measured energy E_d shows the particle identification by giving separate curves for different types of particles. The differences obtained in this way are relatively small however. The following procedure yields some improvement. If the dependence of ε on ρ can momentarily be neglected by taking as an average the curve for $\rho = 0$, it can be stated that for $\tau \leqq 1$ the relation $E_{cl} = \tau_{cl}E_d$ is valid. Thus subtracting αE_d from E_{cl}, $\alpha = \tau_{cl}$, the quantity $E_{cl} - \alpha E_d$ is introduced. This quantity is exactly zero for $\rho = 0$, but it also tends to zero for the real situation $\rho \neq 0$. However since the differences for the various particle types are unaffected by the subtraction, the relative differences are increased. In the experimental work this method was followed.

4. Experimental Arrangement

4.1. BEAM ARRANGEMENT

The experiments were performed with the I.K.O.-synchrocyclotron, which is able to accelerate deuterons to 26 MeV and α-particles to 52 MeV. Most experiments were done with a beam containing deuterons and α-particles simultaneously. High energy protons were obtained from the reaction $^{12}C(d, p)^{13}C$ which gives protons of nearly 29 MeV at small scattering angles, since the Q of the reaction is + 2.72 MeV. An absorber with stepwise varying thickness, drawn schematically in fig. 4, is placed in front of the detector. The various groups of degraded energies, obtained in this way, can be observed in the figs. 6 to 10.

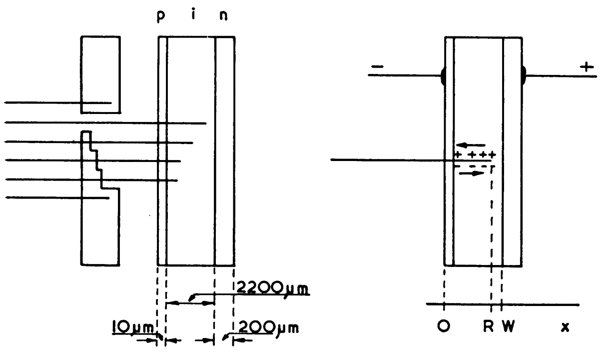

Fig. 4. Schematic representation of the collimator, absorber and detector arrangement. Some quantities related to the detector are also given.

4.2. DETECTOR PROPERTIES

The detector is made according to a standard method published in this journal[2]). Some particular properties of the detector used are:

a. The detector has a circular sensitive area of about 3 cm^2. The beam is collimated by the absorber on a rectangular area of 5 × 5 mm^2 in the centre of this circle.

b. The window-thickness in front of the detector is determined by measurements with the α-particles from a ^{212}Pb-source; after correction for diffusion effects the window-thickness was found to be (10 ± 5)μm.

c. The detector has an intrinsic thickness of 2200 μm at all reverse voltages used in the experiments. Deuterons and α-particles are stopped in the sensitive volume, while the penetration energy for protons lies at 20.3 MeV.

d. The thickness of the insensitive n-type region at the back of the detector is 200 μm.

e. The detector was cooled down to a temperature given by (− 30 ± 10)°C. The temperature could not easily be kept constant. Typical values for the current of the cooled detector are 0.015, 0.03 and 0.06 μA at reverse voltages of 42, 84 and 126 V resp. The detector noise is small compared to the electronic contributions to the noise.

4.3. ELECTRONIC EQUIPMENT

A block diagram of the electronic system is given in fig. 5.

The functions involved in this scheme follow closely the method outlined in § 3.

The signal obtained from the detector is led to a preamplifier, which has a linear characteristic up to high frequencies to avoid distortion of the pulse shape. The first stage, a cascode amplifier consisting of two E810F tubes, is made charge sensitive by feedback through a small capacitance. Further amplification is obtained in a second stage in which transistors of the type 2N769 are used. The whole preamplifier has a rise time of less than 6 ns.

The pulse representing E_d is treated in the lower line of the block diagram. The shaping network contains a single differentiator with a time constant of 10 μs, which improves the energy resolution by suppressing the low frequencies. The signal E_d provides the horizontal bending of the twinkle-box beam.

The signal E_{c1} is formed by delay-line clipping of the preamplifier output pulse at the time t_{c1}. In this way the signal E_{c1} is made equal to the

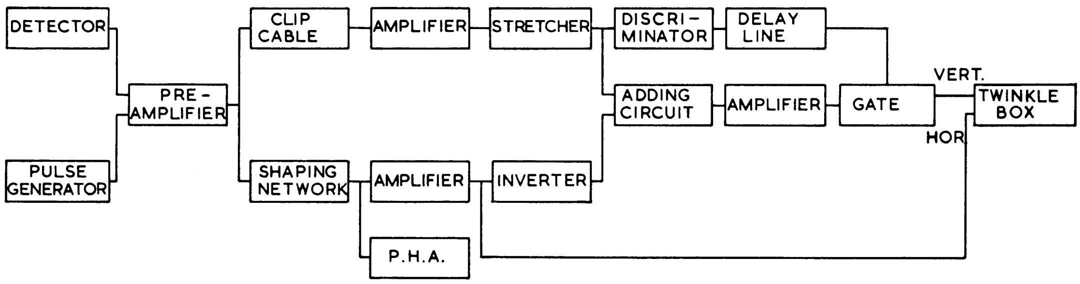

Fig. 5. Block diagram of the electronic equipment.

[2]) C. A. J. Ammerlaan and K. Mulder, Nucl. Instr. and Meth. **21** (1963) 97.

pulse height at $t = t_{cl}$ in accordance with the definition.

In the adding circuit the pulses E_{cl} and inverted E_d come together and the signal $E_{cl} - \alpha_{exp}E_d$ is formed. The parameter α_{exp}, which governs the mixing, is continuously variable over the required range. The signal E_{cl} takes up its correct value at an earlier time than E_d. Thus in order to make a subtraction of the right pulse heights the signal E_{cl} is stretched. A differentiating network causes the tail of the stretched signal to drop off with a characteristic time of 10 μs, the same as for E_d. Also the identifying signal $E_{cl} - \alpha_{exp}E_d$ does not reach its proper value before the pulse rise time has elapsed. Only this value passes the gate at a time somewhat larger than the maximal pulse rise time. It is led to the twinkle-box where it determines the vertical position of the spot. The gate is triggered by the delayed discriminator output pulse.

5. Results

5.1. EXPERIMENTAL RESULTS

As mentioned in § 3 and § 4, sub 4.3. the experimental results appear in the form of twinkle-box pictures. Some of the pictures are reproduced in the figs. 6 to 10. These figures give the identifying quantity $E_{cl} - \alpha_{exp}E_d$ as function of the detected energy E_d. The α-particles are represented by the curves running from 0 to 52 MeV (figs. 6, 7, 8, 10), the deuterons by the curves between 0 and 26 MeV (figs. 6–10). The protons which are stopped in the detector give the curves between 0 and 20.3 MeV; protons with higher energy than the penetration value loose less energy in the detector and are responsible for the lower part in the proton curve which goes down to about 10 MeV (figs. 9, 10). The vertical axis was not calibrated. The parameter α_{exp} was adjusted so as to give a good picture, with roughly horizontal α-particle curve. In this way α_{exp} was made about equal to τ_{cl}; the exact value of α_{exp} is however unknown.

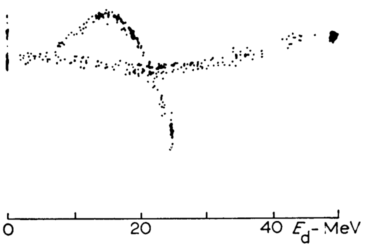

Fig. 6. The separation of deuterons and α-particles. $W = 2200\,\mu$m, $V = 84$ V, $t_{t,e} = 0.36\,\mu$s, $t_{cl} = 0.2\,\mu$s, $\tau_{cl} = 0.56$.

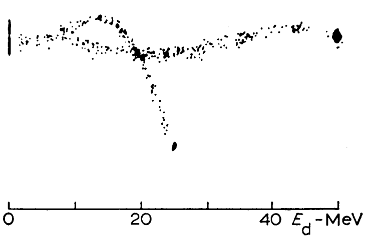

Fig. 7. The separation of deuterons and α-particles. $W = 2200\,\mu$m, $V = 42$ V, $t_{t,e} = 0.72\,\mu$s, $t_{cl} = 0.6\,\mu$s, $\tau_{cl} = 0.83$.

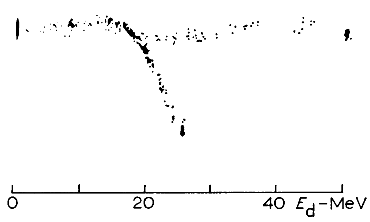

Fig. 8. The separation of deuterons and α-particles. $W = 2200\,\mu$m, $V = 84$ V, $t_{t,e} = 0.36\,\mu$s, $t_{cl} = 0.4\,\mu$s, $\tau_{cl} = 1.11$.

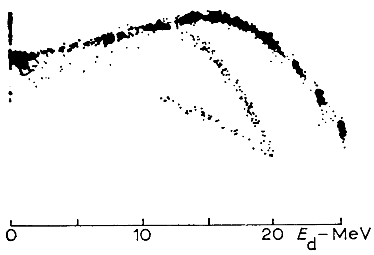

Fig. 9. The separation of protons and deuterons. $W = 2200\,\mu$m, $V = 84$ V, $t_{t,e} = 0.36\,\mu$s, $t_{cl} = 0.3\,\mu$s, $\tau_{cl} = 0.83$.

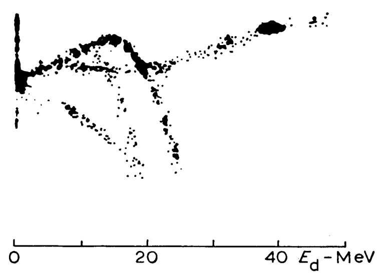

Fig. 10. The separation of protons, deuterons and α-particles. $W = 2200\,\mu$m, $V = 84$ V, $t_{t,e} = 0.36\,\mu$s, $t_{cl} = 0.3\,\mu$s, $\tau_{cl} = 0.83$.

In the figs. 6, 7 and 8 the separation between deuterons and α-particles is shown. The figures 6 and 8 refer to the detector at a reverse bias of 84 V and clipping times of 0.2 and 0.4 resp. The dependence of the reduced pulse height on the reduced range at fixed times during the pulse rise time. These times, with $0 \leqq \tau \leqq 1$, are the times of interest in the particle identification system.

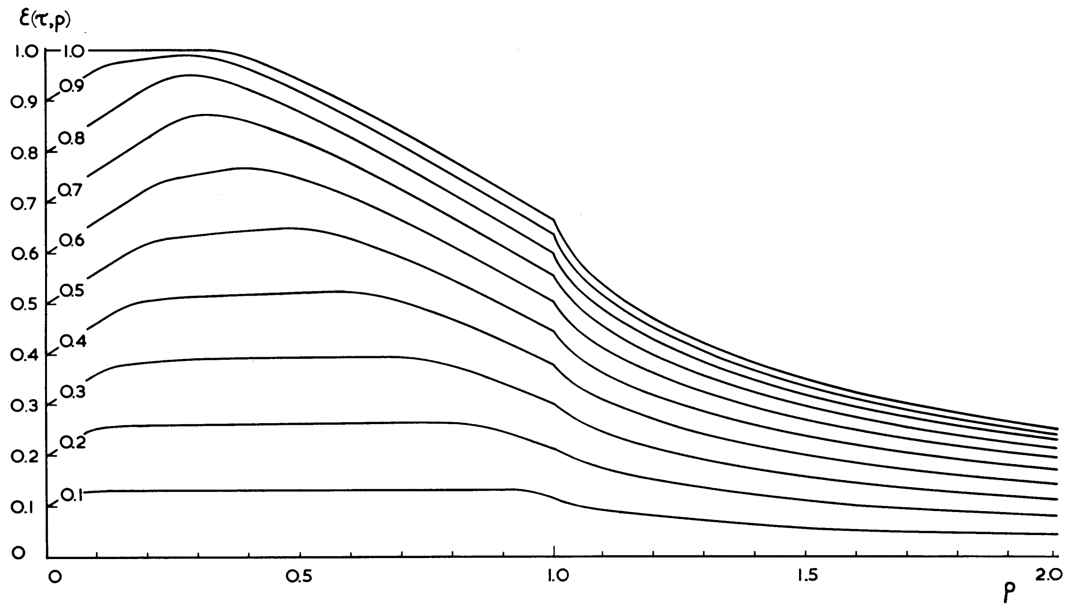

Fig. 11. Pulse analysis showing the dependence of the reduced pulse height on the reduced range for various times during the pulse rise time. The parameter reduced time is indicated on the curves.

picture for the situation $V = 84$ V, $t_d = 0.3$ μs, also available, fits between the figs. 6 and 8, but its publication would have meant a duplication of fig. 10. For this reason the result for the corresponding situation $V = 42$ V, $t_d = 0.6$ μs, having the same τ_{cl}, is given as fig. 7. Although not reproduced, twinkle-box pictures were taken both at higher and at lower values for the clipping time. Similar sets of photographs were also obtained for reverse detector voltages of 42 and 126 V; they yielded equivalent results.

The separation of protons and deuterons is demonstrated by fig. 9, and in fig. 10 all types of particles are shown together.

5.2. CALCULATED RESULTS

All the basic information needed for calculations to check the observed phenomena, is contained in the results of the pulse shape analysis given in § 2. The same data presented in fig. 1 are used for the construction of fig. 11. This figure shows the

From this point the calculations concern only the specific detector thickness $W = 2200$ μm. For each particle type the range R is calculated as function

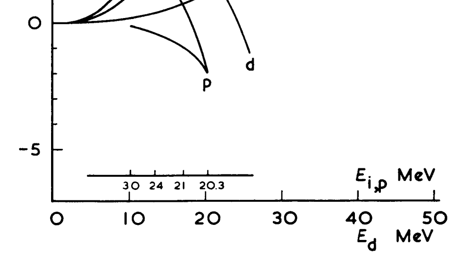

Fig. 12. Analysis of the particle separation for the reduced clipping time $\tau_{cl} = 0.6$; $\alpha_{calc} = 0.6$.

of E_i using the range-energy formula given in § 2. Then ρ is determined. The detected energy E_d, plotted on the horizontal axis, is just equal to E_i in the case $\rho \leqq 1$ and equal to $E_i \{ 1 - (1 - 1/\rho)^{1/1.73} \}$

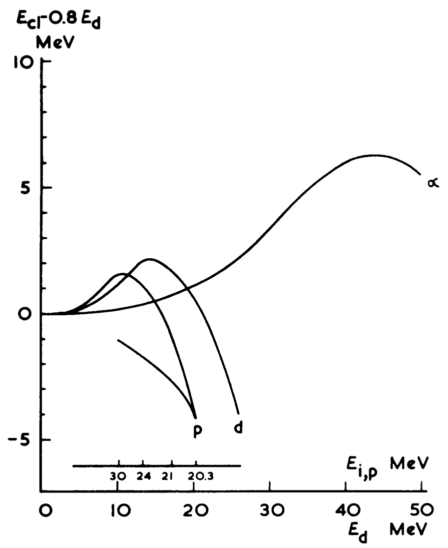

Fig. 13. Analysis of the particle separation for the reduced clipping time $\tau_{cl} = 0.8$; $\alpha_{calc} = 0.8$.

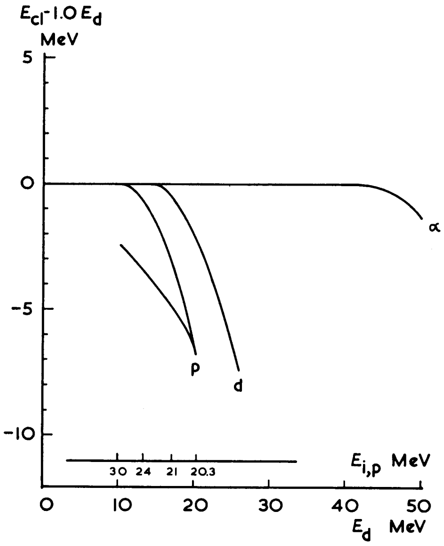

Fig. 14. Analysis of the particle separation for the reduced clipping time $\tau_{cl} = 1.0$; $\alpha_{calc} = 1.0$.

whenever $\rho \geqq 1$. For each clipping time the value of E_{cl}/E_i is read from fig. 11. E_{cl} and E_d are then both known. The quantity corresponding exactly to the experimental identifying signal $E_{cl} - \alpha_{exp} E_d$ cannot be calculated since α_{exp} was not measured. No large errors are made however by approximating α_{exp} with τ_{cl}. Consequently the quantity $E_{cl} - \alpha_{calc} E_d$ is introduced in the calculations where α_{calc} is defined by $\alpha_{calc} = \tau_{cl}$. In the curves, constructed for comparison with the experimental results, $E_{cl} - \alpha_{calc} E_d$ is plotted vertically. The figures 12, 13 and 14 show the final results calculated for $\tau_{cl} = 0.6$, 0.8 and 1.0 resp. The upper horizontal axis refers to protons with energies above the penetration value of 20.3 MeV and gives their incident energy $E_{i,p}$.

6. Discussion

6.1. DETECTOR TEMPERATURE

It was established experimentally that the noise level of the detector was reduced by cooling. The noise, as function of temperature, detector current or frequency could not be understood in terms of shot noise due to space charge generated current. Clearly the edge effects are important.

The mobility of electrons and holes in silicon is temperature dependent, and consequently the pulse rise time will be too. The electron transit time for the case $W = 2200\ \mu$m, $V = 84$ V, $T = 293°$K, is calculated to be 0.48 μs, assuming $\mu_e = 1200$ cm^2/Vs at room temperature. Taking the $T^{-\frac{3}{2}}$ dependence for the electron mobility, which is predicted by lattice scattering theories, the electron transit time is decreased to 0.36 μs at $-30°$C. The reduced clipping times for the experimental situations represented in the figs. 6, 8, 9 and 10 are calculated using this value for $t_{t,e}$; for the situation of fig. 7, $V = 42$ V, the value $t_{t,e} = 0.72\ \mu$s is taken. Faster pulses were observed after cooling of the detector in accord with this explanation.

6.2. EXPERIMENTAL RESULTS VERSUS CALCULATIONS

The results obtained experimentally are in fair agreement with the calculated results. This can be concluded from a comparison of the corresponding figures: 6 and 12; 7, 9, 10 and 13; 8 and 14. A few of the most noteworthy points which clearly demonstrate the similarity are:

a. The position of proton, deuteron and α-particle curves with respect to each other.

b. The E_d-values at the points of intersection between proton and α-particle curves (fig. 10, 13).

c. The E_d-values at the points of intersection between deuteron and α-particle curves as function of τ_{cl} (figs. 6, 7, 8, 12, 13, 14).

d. The energy above which protons and deuterons are separated.

e. The equal values of $E_{cl} - \alpha E_d$ for protons at the break point energy and deuterons at their maximal energy (figs. 9, 10, 13).

The agreement between the experimental and calculated results proves that the operation of the p-i-n detector is quite well understood. Clearly all the assumptions made in § 2 are reasonably valid.

In addition it may be noted that the values of τ_{cl} and α_{exp} in the experimental case are not exactly equal to the values of τ_{cl} and α_{calc} on which the calculations are based. Some slight deviations are explained by these facts.

6.3. PARTICLE IDENTIFICATION PERFORMANCE

The best separation between deuterons and α-particles is obtained for $\tau_{cl} = 0.56$. With exception of the energies around the intersection point at 22 MeV, separation is possible above 8 MeV. The intersection point energy can be shifted upwards by taking smaller clipping times, but only at the cost of the discrimination at lower energies.

The separation at low energies is bad in all cases. This is according to the expectations since the particle identification depends on differences in $E_{cl} = \varepsilon(\tau_{cl}, \rho)E_i$. For low values of ρ no large differences in $\varepsilon(\tau_{cl}, \rho)$ will be found, which means that even the relative effect is small. Moreover at low energies the importance of the window-layer of the detector increases. The stated value of 10 μm is the range of a 3.5 MeV α-particle.

The width of the curves is not sensitive to the detector bias and may be caused by the noise. In this respect no severe attempts have been made to improve the separation.

6.4. THICKER DETECTOR

Some experiments, with deuterons and α-particles, were carried out with an other p-i-n detector with larger intrinsic thickness: $W = 4400$ μm. Since the largest range, that of 26 MeV deuterons, is about 2000 μm only the first half of the detector is utilized. The main differences with the mentioned results for the detector with $W = 2200$ μm are:

a. The separation at the lower energies is somewhat less. This is explained by the fact that the same differences in the range R result in differences in the reduced range ρ which are half as great, since W is twice as large.

b. The curves for reduced clipping times around $\tau = \frac{3}{4}$ do not intersect each other. The intersection points, obtained by extrapolation of the deuteron curves above 26 MeV, agree with the results of the calculations made for this detector.

6.5. RADIATION ON THE n-SIDE

It was expected that better results could be obtained for particles incident on the n-side of the detector. The expectation was based on the fact that in this case the slower holes generally have to traverse the longer distance. This implies that the pulse becomes faster monotonic when the range increases. This is in contrast with the situation for radiation incident on the p-side of the detector. In this case, as shown in fig. 11, ε_{cl} first increases as function of ρ up to about $\rho = \frac{1}{3}$, and then decreases. This unfavourable property causes the intersection of the curves.

Consequently the case of radiation incident on the n-type side of the detector has been considered theoretically too. A pulse shape analysis, analogous to that given in § 2, was made and graphs, like those given in fig. 12 to 14, were constructed. These graphs indeed show that better separation is obtained. The phenomenon of the intersecting curves has disappeared almost completely and can be avoided easily.

No experiments were carried out with radiation incident on the n-side of a detector. At the time no detector with an insensitive window-layer on this side of less than 150 μm was available.

6.6. TIMING METHOD

A second method to obtain particle separation was also investigated. In this procedure an attempt was made to determine the time at which the last hole reaches the front electrode, by twice differentiating the voltage signal from the detector. This time, equal to $RW/\mu_h V$, is proportional to the range of a particle and may replace E_{cl}. Although the separation between deuterons and α-particles obtained by this method and by the method of pulse clipping were comparable, the results were unintelligible. This was probably due to imperfections in the somewhat improvised electronic equipment.

6.7. ONE DETECTOR

A well developed method for the identification of charged particles at the energies considered in this paper is the system by which the energy and the energy loss per unit length dE/dx are measured in two separate detectors. Using these quantities in suitable analog computations an output pulse is obtained, which independent of the particle energy, is characteristic for the particle type[3]). The particle separation obtained with this method is superior to the first results given in this paper. An advantage of the method based on pulse shape discrimination is that the need for a thin detector is avoided and consequently its noise is eliminated.

[3]) F. Udo, R. F. Rumphorst and L. A. Ch. Koerts, Nuclear Electronics II, (I.A.E.A., Vienna, 1962) p. 413.

Acknowledgements

The authors express their thanks to Prof. P. C. Gugelot for his kind interest in the work. The method for the preparation of p-i-n detectors was developed in close cooperation with K. Mulder, while J. Joosten assisted in the actual production of the detectors. We give special thanks to the cyclotron operators who adjusted the mixture of deuterons and α-particles to the demand of the experiment.

The experiments were performed as part of the research program of the Institute for Nuclear Physics Research, made possible by financial support from the Foundation for Fundamental Research of Matter (F.O.M.) and the Dutch Organisation for Pure Scientific Research (Z.W.O.).